Nanoscale Advances

ROYAL SOCIETY OF CHEMISTRY

PAPER

View Article Online
View Journal | View Issue

Cite this: *Nanoscale Adv.*, 2020, **2**, 5728

Nanonewton forces between *Staphylococcus aureus* surface protein IsdB and vitronectin†

Marion Mathelié-Guinlet, [a] Felipe Viela, [a] Giampiero Pietrocola, [b] Pietro Speziale *[b] and Yves F. Dufrêne *[ac]

Single-molecule experiments have recently revealed that the interaction between staphylococcal surface proteins and their ligands can be extremely strong, equivalent to the strength of covalent bonds. Here, we report on the unusually high binding strength between *Staphylococcus aureus* iron-regulated surface determinant B (IsdB) and vitronectin (Vn), an essential human blood protein known to interact with bacterial pathogens. The IsdB–Vn interaction is dramatically strengthened by mechanical tension, with forces up to 2000 pN at a loading rate of 10^5 pN s^{-1}. In line with this, flow experiments show that IsdB-mediated bacterial adhesion to Vn is enhanced by fluid shear stress. The stress-dependent binding of IsdB to Vn is likely to play a role in promoting bacterial adhesion to human cells under fluid shear stress conditions.

Received 2nd August 2020
Accepted 16th October 2020

DOI: 10.1039/d0na00636j

rsc.li/nanoscale-advances

Staphylococcus aureus, a human commensal of the microbiota frequently colonizing the respiratory tract and the skin,[1,2] is also an opportunistic pathogen causing a range of illnesses from minor skin and respiratory infections to life-threatening diseases such as endocarditis and sepsis.[2–4] In the past decades, due to its key role in nosocomial infections and to the emergence of antibiotic-resistant strains, *S. aureus* has become a worldwide clinical problem.[2,5] *S. aureus* can invade a variety of mammalian cells, from endothelial[6,7] and epithelial cells[8–10] to osteoblasts,[11,12] thereby enabling it to evade host immune defenses. Attachment of bacterial pathogens to host cells and biomaterials is the first step leading to infection. Key players in cell adhesion are bacterial adhesins which specifically bind to host surfaces and proteins from the extracellular matrix (ECM).[13] Among these, vitronectin (Vn) plays major roles in bacterial pathogenesis by supporting complement escape to the immune system, adhesion and cellular invasion.[14,15] Vn is a ~75 kDa (sequence ~ 450 residues) multifunctional glycoprotein found as folded monomers in the plasma and as multimers in the ECM.[16] It comprises a somatomedin-B domain, followed by an RGD sequence, four hemopexin-like repeats and three heparin-binding domains (Fig. 1A).[16,17]

S. aureus can bind Vn with high-to-moderate affinity (10^{-10} to 10^{-8} M) depending on the bacterial recognition sites involved.[18–20] Many microbial pathogens, including *S. aureus* were found to bind human Vn *via* the same C-terminal heparin-binding domain, leaving the complement regulatory region of Vn accessible and subsequently allowing versatile host immune responses.[21,22] Of note, similarly to *Moraxella catarrhalis* and *Haemophilus influenzae*[14] both multimeric and monomeric forms of Vn have the capability to interact with *S. aureus*. But, multimeric forms of Vn bind to *S. pneumoniae* and *S. aureus* more efficiently than monomeric forms, likely due to better exposition of bacterial binding-sites in such conformations.[23–26] Furthermore, Vn also enhances staphylococcal adhesion to biomaterials like catheters.[27]

Staphylococci express iron-regulated surface determinant (Isd) proteins that are upregulated under iron-restricted conditions.[28,29] These proteins, whose main task is to bind hemoglobin and extract heme to provide the cell with a source of iron, contain one to three near iron transporter (NEAT) motifs (Fig. 1A). These domains consist of ~120 amino acids with a conserved eight-stranded beta-sandwich fold that mediates the binding to hemoproteins or heme through an hydrophobic pocket.[30] In addition, Isd proteins are involved in adhesion, colonization and pathogenesis.[31] For instance, IsdA and IsdB were shown to promote adhesion to squamous epithelial cells and platelets respectively, and their subsequent invasion.[32,33] IsdC from *Staphylococcus lugdunensis* increases adhesion to abiotic surfaces but also in between cells, subsequently favoring biofilm formation.[34] Zapotoczna *et al.* suggested that *S. aureus* IsdB interacts with specific integrins that bind ligands with an RGD motif, improving further cell invasion.[35] Vn is one such ligand which has distinct RGD sequences

[a]*Louvain Institute of Biomolecular Science and Technology, UCLouvain, Croix du Sud, 4-5, bte L7.07.07, B-1348 Louvain-la-Neuve, Belgium. E-mail: yves.dufrene@uclouvain.be*

[b]*Department of Molecular Medicine, Unit of Biochemistry, University of Pavia, Viale Taramelli 3/b, 27100 Pavia, Italy. E-mail: pietro.speziale@unipv.it*

[c]*Walloon Excellence in Life Sciences and Biotechnology (WELBIO), B-1300 Wavre, Belgium*

† Electronic supplementary information (ESI) available. See DOI: 10.1039/d0na00636j

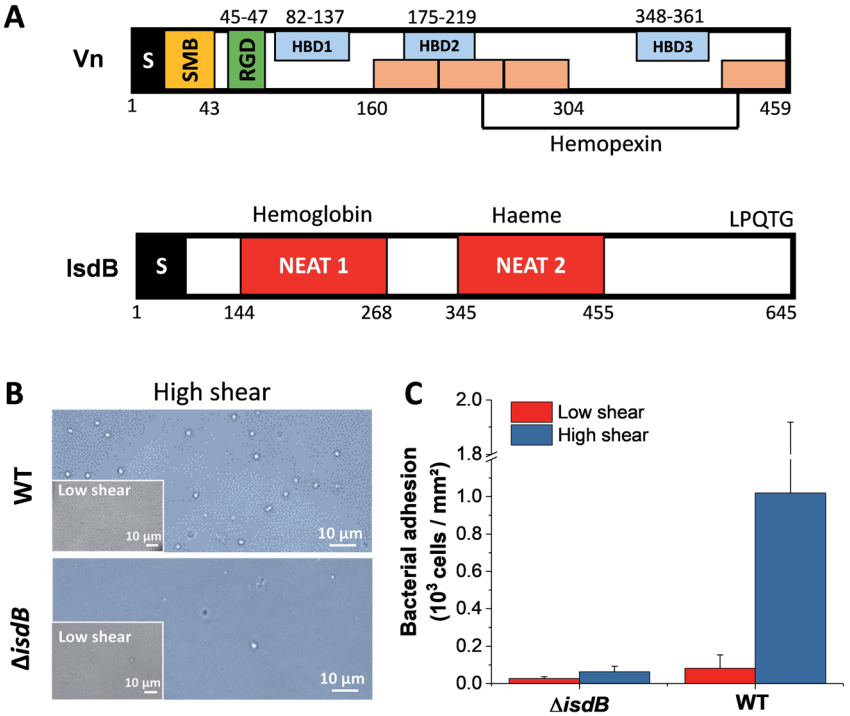

Fig. 1 IsdB-dependent bacterial adhesion to Vn-substrates. (A) Schematic diagram of the domain organization of Vn and IsdB. S: signal sequence; SMB: somatomedin B domain; HBD: heparin-binding domain; NEAT: near iron transporter domain. Orange boxes are the hemopexin-like domains, predicted as putative haem-binding motifs in Vn. (B) Bacterial adhesion to Vn increases with fluid shear stress. Optical microscopy images of WT and Δ*isdB* bacteria adhering to Vn-coated surfaces in a microparallel flow chamber, under low and high shear stress. Shown in (*C*) is the quantification of the amounts of adhering bacteria (from a total of 6 images from 3 experiments for each condition).

and bacterial-binding domains.[14] It has therefore been suggested that IsdB stabilizes Vn-binding integrins, allowing more vitronectin to bind.[35]

IsdB has been shown to act as a receptor for Vn (multimeric and monomeric conformation), under iron starvation conditions under which those adhesins are expressed at the surface of *S. aureus*.[36] Adherence to and subsequent invasion of mammalian cells were then promoted by the bridge Vn can form between IsdB and $\alpha_v\beta_3$ integrin on the host cell. Despite the potential role of Vn-binding by Isd proteins in *S aureus* pathogenesis, the molecular details of such interaction and the adhesins involved have not yet been elucidated. Here we demonstrate that IsdB and Vn form molecular complexes with very high mechanical stability, which is achieved under high physical stress.

Results

IsdB mediates strong bacterial adhesion to Vn-coated surfaces

We first tested the ability of *S. aureus* SH1000 to bind to Vn using a macroscopic adhesion assay, where bacterial suspensions were flowed over Vn-coated substrates mounted into a microparallel flow chamber. As *S. aureus* can encounter Vn in the bloodstream, allowing for a better colonization of endothelial cells, bacterial adhesion was first studied under flow at low and high shear stress, 12 and 120 s^{-1} respectively lying in the moderate range of physiological values which can broadly vary depending on blood vessels[37] (Fig. 1B and C). Adhering bacteria were quantified by direct observation by optical microscopy. While WT bacteria poorly adhered at low shear rate, adhesion was largely increased at high shear rate, corresponding to normal venous shear rates. Mutant cells lacking IsdB poorly adhered whatever the flow conditions. This shows that IsdB supports *S aureus* adhesion to Vn surfaces under fluid flow, in a shear stress dependent manner.

This prompted us to study the molecular interactions between IsdB and Vn using AFM. Force–distance curves were recorded by performing approach–retract cycles between single bacteria immobilized on an AFM colloidal probe and a defined area (5 μm × 5 μm) of Vn-coated substrates (single-cell force spectroscopy, SCFS, Fig. 2, for more cells see ESI Fig. 1†). From those pixel-by-pixel force–distance maps, adhesion events were determined. For three representative cells, many force curves (39%, mean from 3 cells; Fig. 2A) featured adhesion events with small forces centered at 155 ± 96 pN (mean ± s.d.; $n = 531$ adhesive curves; 3 cells). Of note, a few adhesion events (~10%) of 1026 ± 450 pN (mean ± s.d.; $n = 67$ adhesive curves; 3 cells) were also observed. Mutant cells lacking IsdB poorly adhered to Vn, with lower forces (Fig. 2B): the adhesion probability decreased significantly from 37% to 24% (mean from 11 and 7 cells for WT and Δ*isdB* respectively; Fig. 4A) – supporting the specificity of the forces measured with the WT. Nonetheless the residual adhesion observed with mutant cells might reflect interactions with other Vn-receptors or unspecific attachment.

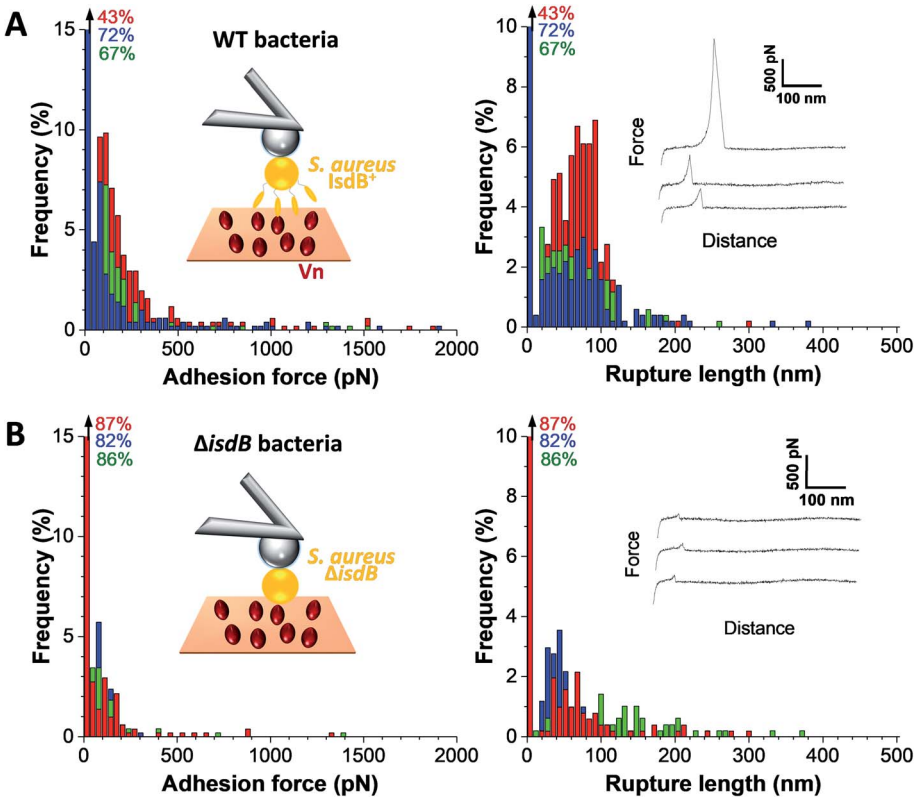

Fig. 2 Adhesion forces between single bacteria and Vn-substrates. Maximum adhesion force (left) and rupture length (right) histograms with representative retraction force profiles (right insets) obtained by recording force–distance curves in PBS, at a retraction speed of 1 μm s^{-1} (~2 × 10^4 pN s^{-1}), between three (A) WT and (B) Δ*isdB S. aureus* cells and Vn substrates (n = 599 and n = 220 adhesive curves for WT and mutant cells respectively). Percentages shown in the upper left corner of each histogram corresponds to the non-adhesive events. Left insets represent schemes of the single-cell force spectroscopy setup.

It is worth mentioning that such a decrease cannot be explained by either Vn being ripped from the substrate or IsdB/Vn being removed from their corresponding surface because of the EDC/NHS chemistry used and the constant binding probability over time respectively.

Bacterial-Vn interactions ruptured at 73 ± 41 nm (mean ± s.d.; n = 531 adhesive curves; 3 cells). Vn molecules were immobilized on the substrates through multiple sites, meaning they should not substantially contribute to the measured extensions. Mature IsdB is made of ~600 residues; assuming that each amino acid contributes 0.36 nm, the fully unfolded protein should be ~215 nm. This suggests that bonds rupture before complete unfolding of IsdB, thus suggesting the protein is mechanically stable.

Strength and dynamics of the IsdB–Vn interaction

The strength of single IsdB–Vn bonds was then studied by pulling on single IsdB adhesins on top of the living bacteria immobilized on a polystyrene dish with AFM tip functionalized with Vn, in a similar pixel-by-pixel force–distance maps (single-molecule force spectroscopy, SMFS, Fig. 3, for more cells see ESI Fig. 2†). Consistent with SCFS experiments, weak forces of 137 ± 117 pN (mean ± s.d.; n = 271 adhesive curves; 3 cells) were observed for representative WT cells but also much larger ones, ranging from 500 pN to 2000 pN (~25% of adhesive events) (Fig. 3A). Similar force distributions were obtained both in SCFS and SMFS (Fig. 4C and D): (i) in the low force regime, mean forces of 125 ± 23 pN (probability of 92%, n = 11 cells) and 101 ± 41 pN (probability of 86%, n = 13 cells) were respectively reported while (ii) in the high force regime, mean forces of 870 ± 117 pN (probability of 8%, n = 11 cells) and 1028 ± 155 pN (probability of 17%, n = 13 cells) were respectively observed. This, along with the single-peak nature of adhesion events (see retraction profiles in Fig. 2 and 3) and the absence of clear multiples of a single adhesion force unit, support the idea that we are probing single bonds rather than multiple bonds rupturing in parallel. Again, binding was specific as most adhesion events were abrogated with the mutant lacking IsdB (Fig. 3B), for which the adhesion probability dropped from 11% (mean on 12 WT cells) to 6% (mean on 10 Δ*isdB* cells) (Fig. 4B). The rupture lengths were 63 ± 44 nm, which is smaller than the length of unfolded adhesins (~210 nm), again confirming the rupture before complete unfolding. Finally, we also probed recombinant IsdB proteins, showing that, overall, they feature similar binding force properties for Vn (Fig. 3C). However, on closer examination we found that strong forces > 500 pN were hardly observed. This suggests that when adhesins are randomly attached on a surface they cannot engage into strong bonds, unlike when they are natively oriented on living bacteria.

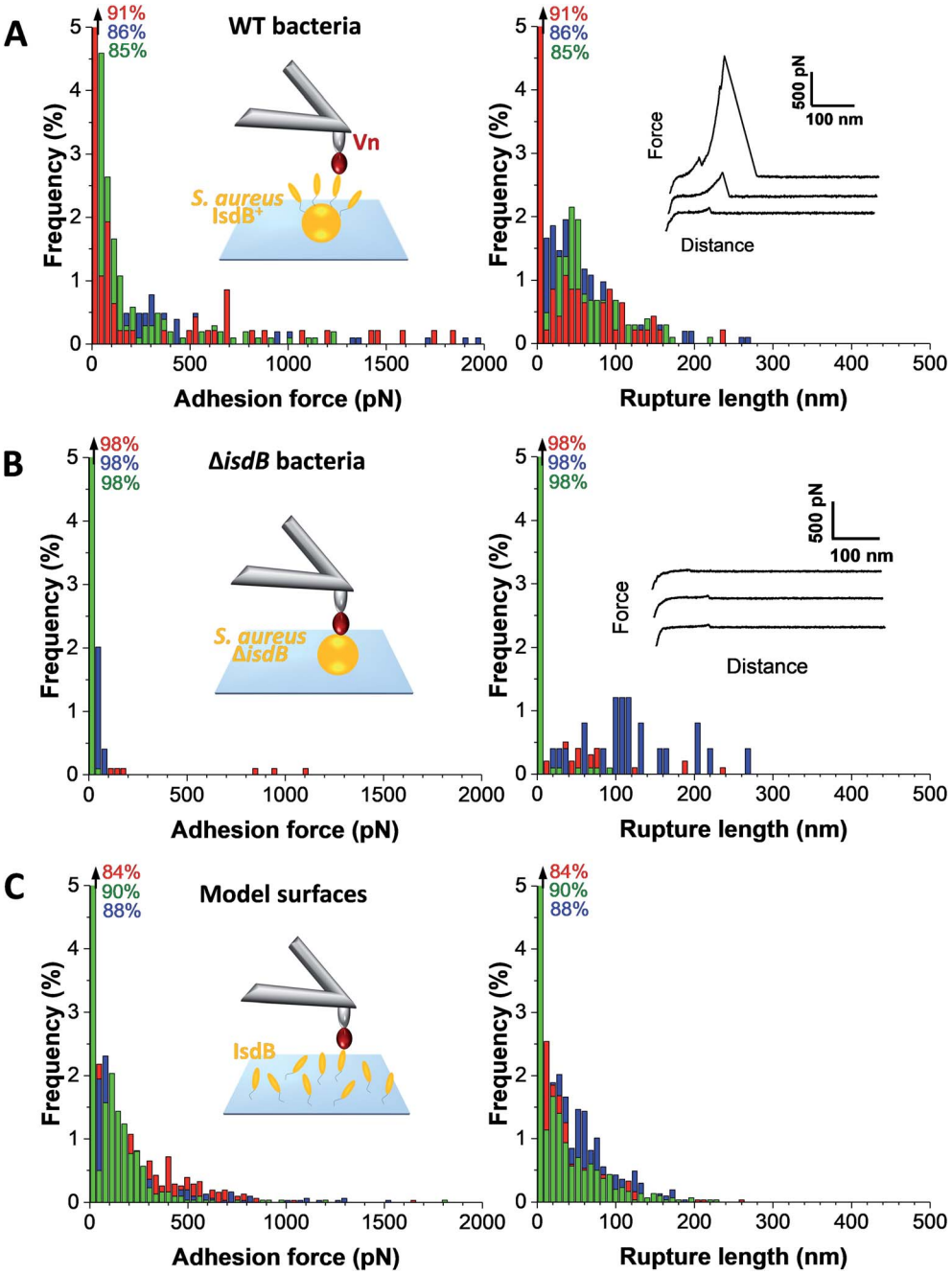

Fig. 3 Strength of single IsdB–Vn interactions. Maximum adhesion force (left) and rupture length (right) histograms obtained by recording force–distance curves in PBS, at a retraction speed of 1 μm s^{-1} (~2 × 10^4 pN s^{-1}), between three different WT (A) or Δ*isdB* (B) *S. aureus* cells and AFM tips functionalized with Vn, along with representative retraction force profiles (right insets) (n = 357 and n = 64 adhesive curves for WT and mutant cells respectively). Left insets represent schemes of the single-molecule force spectroscopy setup. (C) Same force and rupture length histograms obtained, on three independent samples, between AFM tips functionalized with Vn and IsdB-coated substrates (n = 310 adhesive curves). Percentages shown in the upper left corner of each histogram corresponds to the non-adhesive events.

Bacterial adhesion is strongly influenced by physical stress like fluid flow.[38,39] To sustain these mechanical forces, *S. aureus* express a series of surface adhesions that firmly bind to host cells and ECM proteins.[40] SdrG, ClfA, and ClfB have been shown to bind their ligands through ultrastrong forces, activated by mechanical tension.[41–43] To test whether this also happens with IsdB, the adhesion force between Vn tips and IsdB cells was measured at different retraction speeds (from 0.5 μm s^{-1} to 10 μm s^{-1}, see ESI Fig. 3†), in turn different loading rates (LRs), estimated from the force *vs.* time curves (Fig. 5A). As exemplified for one representative cell, (i) no significant dependency was found between adhesion force and rupture length, at a defined retraction speed, and (ii) the rupture length distributions (and average values) obtained when probing the cell at

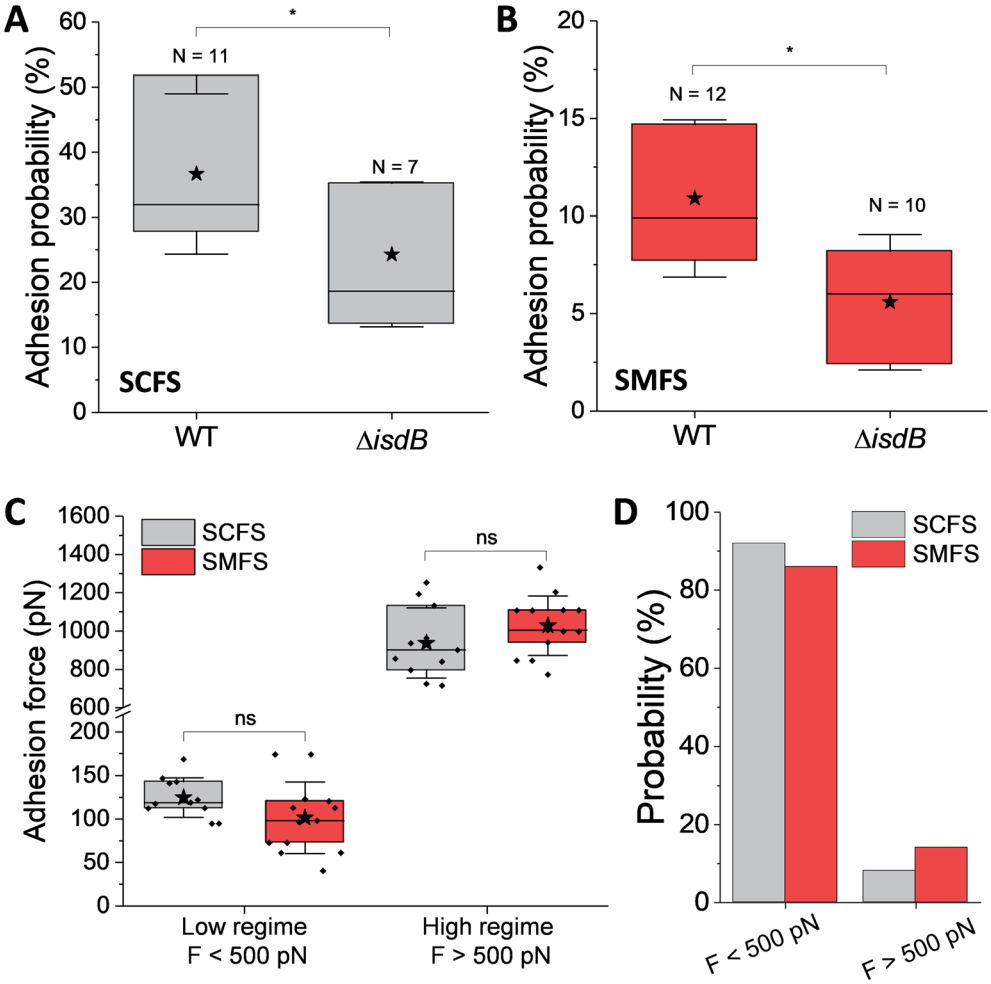

Fig. 4 Comparison of single-cell and single-molecule measurements. (A and B) Box plots showing the adhesion probability of WT and Δ*isdB* cells to Vn, obtained on N independent cells, in single-cell (SCFS) and single-molecule (SMFS) force spectroscopy respectively. (C) Mean adhesion forces reported in both the low ($F < 500$ pN) and high ($F > 500$ pN) force regimes. Stars are the mean values, boxes the 25–75% quartiles and whiskers the SD. For statistical differences, based on Student *t*-tests: $*p \leq 0.05$ and ns is no significant difference. (D) Probability of observing the low and high forces both in SCFS and SMFS.

different speeds were not significantly different (ESI Fig. 3†). We are thus confident that the same adhesion events are probed along the loading rate variations. Then, unbinding forces were analyzed over discrete ranges of LRs (Fig. 5B, see also ESI Fig. 4†). While adhesion forces showed a spread distribution neither described by the classical Bell Evans[44] or Friddle-Noy-De Yoreo[45] models, these measurements revealed that only weak forces of 51 ± 45 pN were observed at low LRs (<3500 pN s^{-1}), while strong forces of 506 ± 538 pN dominated at high LRs (>3500 pN s^{-1}). It is worth mentioning that, at the highest LRs probed here, the measured forces might actually be underestimated by ~10% due to the cantilever dynamics, meaning that the actual "true" rupture forces might even be higher at the highest LRs.[46] Though it is difficult to uncorrelate the mechanical tension exerted on the bond from the actual measurement of the rupture force, it is clear that the probability of observing strong rupture forces increases with the LR, while the population of lower forces becomes depleted (ESI Fig. 4†). Such shift towards higher forces, both in terms of probability and strength suggests a strengthening of the IsdB–Vn bond with tensile force. This behavior is fully consistent with the higher adhesion of IsdB bacteria to Vn-coated surfaces when the shear rate is increased (Fig. 1C). Finally, we assessed the spring constant of the molecular complex (k_m) using the slope of the linear portion of the force *vs.* tip position curves (Fig. 5C). Compared to weak forces, strong forces > 500 pN were associated with higher molecular stiffness ($k_m = 4.2 \pm 3.9$ pN nm^{-1} *vs.* $k_m = 35.3 \pm 22.3$ pN nm^{-1} respectively; mean ± s.d. over 6 cells). Altogether our data suggest that the shift towards strong forces results from a change in the conformational state of IsdB, from a weak- to a strong-binding state, as observed for catch bonds.

Discussion

The structure of IsdB is unique in that it contains two NEAT motifs, structurally solved, that bind to hemoglobin or haem.[16] While IsdA which has one such motif binds multiple ligands – haem, fibrinogen, fibronectin, cytokeratin 10, and loricrin –,[47]

the ligand-binding activities of IsdB are much less understood. IsdB promotes adhesion to human cells as well as platelets,[35] but whether this involves specific ligand interactions is currently unknown. Recently, IsdB has been identified as a specific, high affinity Vn-binding protein and both NEAT motifs of the protein individually bind Vn with an affinity in the nanomolar range.[36] Furthermore, IsdB binding to Vn was specifically inhibited by heparin and high concentrations of NaCl. Biological implications of such interaction involve the interference of IsdB-bound Vn with the assembly and deposition of the terminal complement complex on the bacterial surface and adherence to and invasion of epithelial and endothelial cells by *S. aureus*. We have shown here that IsdB and Vn form molecular complexes that are extremely stable, eventually reaching high strength in the nN regime. We expect this interaction to be of biological importance as Vn plays multiple functions in bacterial pathogenesis, including mediating complement escape, bacterial adherence, and cellular invasion.[14]

The probability of forming strong bonds increases with the rate of applied force, strong IsdB–Vn adhesion being only observed at high tensile load. In line with this, macroscopic adhesion assay demonstrate higher bacterial adhesion levels at increased shear stress. As previously hypothesized in the case of the prototypical strong SdrG–Fg bonds,[48] such force-enhanced activity is reminiscent of a catch bond behavior, *i.e.* the counterintuitive capacity of a bond to be longer-lived under high external stress than under low stress, as opposed to the increasing shorter-lived slip bonds. The transition from weak to strong interaction correlates with an increase in molecular stiffness. For the mechanically stable multidomain cellulosome protein complex,[49] steered molecular dynamics and single-molecule experiments revealed that strong forces (600–750 pN) can be achieved if the complex directs force along pathways nonparallel to the pulling direction. This supports a model whereby force induces conformational changes in the adhesin, from a weak-binding folded state, to a strong-binding extended state. We speculate that IsdB might sense mechanical forces acting on the cell surface and induce intracellular responses.

Vn is present in the ECM and in soluble form in biological fluids and shows similarity, in terms of adhesion properties, with fibrinogen (Fg) and fibronectin (Fn). It is thus interesting that our finding of a strong interaction triggered by mechanical force is qualitatively similar to what has been recently described for the some staphylococcal adhesins binding either Fg or Fn through DLL[41–43,48] and β-zipper[50,51] mechanisms. The strong DLL interaction results from an intricate hydrogen bond network between the ligand peptide backbone and the N2N3 subdomains.[48] Under load, the screw-like arrangement of hydrogen bonds maintains the peptide in a perfect shear geometry. In the β-zipper interaction, the well-studied FnBPA–Fn interactions involve the binding of Fn-binding repeats (FnBRs) to Fn-FI modules, subsequently forming additional β-strands along triple peptide β-sheets in the Fn molecule.[51]

What is the molecular basis of the IsdB–Vn interaction? Hallströmet *et al.* found that several pathogens recognize Vn, *via* the same C-terminal heparin-binding domain (amino acids

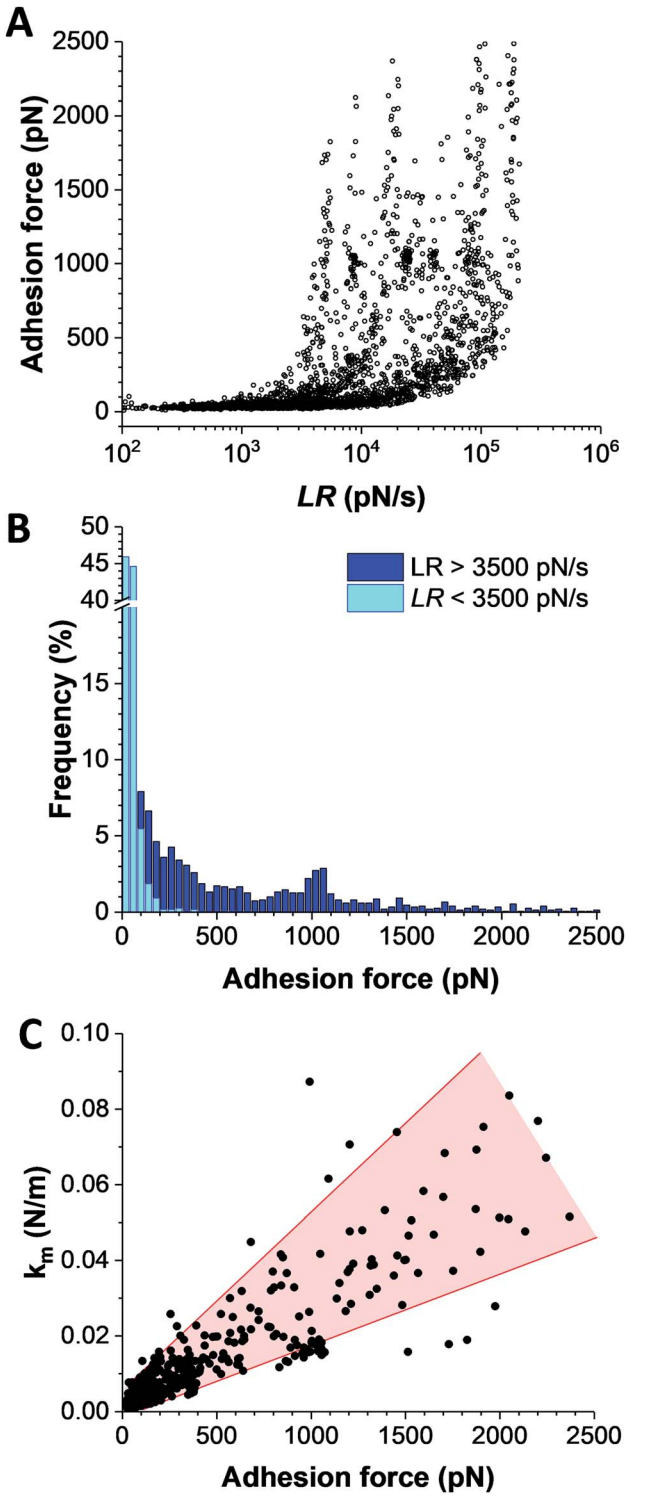

Fig. 5 Physical stress strengthens the IsdB–Vn interaction. (A) Dynamic force spectroscopy data showing the adhesion forces for IsdB–Vn interactions measured at increasing LRs on WT *S. aureus* cells ($n = 2666$ data points from 6 independent cells). (B) Force distributions plotted as histograms depending on two ranges of LRs, suggesting that the probability of forming strong bonds increases with the LR. (C) Plot of the spring constants of the molecular complex (k_m) as a function of adhesion force.

352–374).[21] This allowed microbes to utilize the complement inhibitory function of Vn, as the N-terminal functional region of vitronectin was not shielded. This contributes to evasion of direct lysis by complement, which is an important step in pathogenesis. We therefore speculate that both NEAT domains of IsdB bind the C-terminal site of Vn, as already proposed by Pietrocola *et al.*[36]

That ligand-binding is strengthened by mechanical force highlights the importance of physical stress in activating *S. aureus*–hosts interactions.[52] In the human body, the pathogen can be exposed to variable amounts of Vn as well as different shear stress conditions. Notably, Vn is abundantly present in periodontal, lung and kidney tissues while being less available in skin and gastrointestinal tissues. The stress-dependent IsdB–Vn adhesion may thus help the bacteria to efficiently colonize host cells through weak or strong interactions depending on the physical stress they experience.

Experimental procedures

Bacterial strains and growth conditions

S. aureus SH1000 (both WT and Δ*isdB* cells) were first grown in Brain Heart Infusion (BHI) broth overnight, at 37 °C and under shaking at 200 rpm, to reach their stationary phase. They were then diluted 100× and grown in RPMI overnight (37 °C, 200 rpm) to create iron-restricted conditions. For AFM experiments, cells were harvested by centrifugation at 3000 × *g* for 5 minutes and washed twice with PBS. Construction of *S. aureus isdB* deletion mutant was performed as reported previously.[35]

Isolation of Vn from human plasma

Human Vn was purified from human plasma on a heparin-Sepharose Hi-TrapTM column (GE Healthcare) following the protocol reported by Pietrocola *et al.*[36]

Functionalization of substrates and cantilevers with Vn

Gold-coated glass coverslips and cantilevers (OMCL-TR400PB-1, Olympus Ltd., Tokyo, Japan; nominal spring constant ∼ 0.02 N m^{-1}) were immersed overnight in an ethanol solution containing 1 mM of 10% 16-mercaptododecahexanoic acid/90% 1-mercapto-1-undecanol (Sigma), rinsed with ethanol and dried with N2. Substrates and cantilevers were then immersed for 30 min into a solution containing 10 mg mL^{-1} *N*-hydroxysuccinimide (NHS) and 25 mg mL^{-1} 1-ethyl-3-(3-dimethylaminopropyl)-carbodiimide (EDC) (Sigma) and rinsed with Ultrapure water (ELGA LabWater). Finally, they were incubated with 0.1 mg mL^{-1} of Vn for 1 h, rinsed further with PBS buffer, and then immediately used without dewetting.

Bacterial adhesion to vitronectin-coated surfaces

For flow experiments, *S. aureus* bacterial suspensions were flowed over vitronectin-coated surfaces for 2 min. using a fluidic chamber and a peristaltic pump (Miniplus, Gilson).[53] Two different flow rates were tested, 2 and 20 mL min^{-1}, corresponding to shear rates of 12 and 120 s^{-1} respectively that match the ones encountered in veins.[37] Loosely attached bacteria were removed by flowing PBS during 2 min using the corresponding flow rates. Adhering bacteria were imaged using an inverted microscope (Leica DM16000) and counted using the ImageJ image analysis software (NIH Image).

Single-cell force spectroscopy

Colloidal probes were prepared as described earlier.[54] Briefly, single silica microsphere (6.1 μm diameter, Bangs laboratories) were attached with a thin layer of UV-curable glue (NOA 63, Norland Edmund Optics) on triangular shaped tip-less cantilevers (NP-O10, Bruker). Those newly modified cantilevers were then immersed for 1 h in Tris-buffered saline (TBS; Tris, 50 mM; NaCl, 150 mM; pH 8.5) containing 4 mg mL^{-1} dopamine hydrochloride (Sigma-Aldrich), rinsed in TBS, and directly used to catch single cells. The spring constant was finally determined by the thermal noise method and gave $k \sim 0.08$ N m^{-1}. For single-cell experiments, 100 μL of a suspension of 1×10^6 cells were dropped on a glass Petri dish, next to a Vn-coated substrate, the whole being immersed in PBS. The colloidal probe was brought into contact with a bacterium and retracted to catch the cell through electrostatic interactions with polydopamine. The cell probe was then positioned over Vn-substrates without dewetting. Cell probes were used to measure interaction forces on Vn-surfaces at room temperature by recording multiple forces curves (16 × 16) on different spots, a maximum applied force of 250 pN, and approach and retraction speeds of 1 μm s^{-1} and a contact time of 500 ms. Data were analyzed with the data processing software from JPK Instruments (Berlin, Germany). Adhesion force and rupture distance histograms were obtained by calculating the adhesion force and rupture distance of the last peak for each curve.

Single-molecule force spectroscopy

For SMFS experiments, cantilevers ($k \sim 0.02$ N m^{-1}) were prepared as described above and bacteria were immobilized on polystyrene substrates. SMFS measurements were performed at room temperature in PBS buffer with a NanoWizard IV atomic force microscope (JPK Instruments). Adhesion maps were obtained by recording 32 × 32 force–distance curves on areas of 500 by 500 nm^2 with an applied force of 250 pN, a constant approach and retraction speed of 1 μm s^{-1} and a contact time of 500 ms. SMFS data were processed and analyzed the same was as for SCFS experiments.

Author contributions

MMG, FV, GP, PS and YFD designed the experiments, analysed the data and wrote the article. MMG and FV collected the data.

Conflicts of interest

There are no conflicts of interest to declare.

Acknowledgements

Work at the Université catholique de Louvain was supported by the European Research Council (ERC) under the European Union's Horizon 2020 research and innovation programme (grant agreement no. 693630), the FNRS-WELBIO (grant n°WELBIO-CR-2015A-05), the National Fund for Scientific Research (FNRS), and the Research Department of the Communauté française de Belgique (Concerted Research Action). Y. F. D. is Research Director at the FNRS.

References

1 A. L. Byrd, Y. Belkaid and J. A. Segre, *Nat. Rev. Microbiol.*, 2018, **16**, 143–155.
2 C. P. Parlet, M. M. Brown and A. R. Horswill, *Trends Microbiol.*, 2019, **27**, 497–507.
3 D. C. Angus and T. van der Poll, *N. Engl. J. Med.*, 2013, **369**, 840–851.
4 L. Thomer, O. Schneewind and D. Missiakas, *Annu. Rev. Pathol.: Mech. Dis.*, 2016, **11**, 343–364.
5 P. Moreillon and Y.-A. Que, *Lancet*, 2004, **363**, 139–149.
6 S. K. Ogawa, E. R. Yurberg, V. B. Hatcher, M. A. Levitt and F. D. Lowy, *Infect. Immun.*, 1985, **50**, 218–224.
7 B. E. Menzies and I. Kourteva, *Infect. Immun.*, 1998, **66**, 5994–5998.
8 K. W. Bayles, C. A. Wesson, L. E. Liou, L. K. Fox, G. A. Bohach and W. R. Trumble, *Infect. Immun.*, 1998, **66**, 336–342.
9 K. Dziewanowska, J. M. Patti, C. F. Deobald, K. W. Bayles, W. R. Trumble and G. A. Bohach, *Infect. Immun.*, 1999, **67**, 4673–4678.
10 B. Sinha, P. P. François, O. Nüße, M. Foti, O. M. Hartford, P. Vaudaux, T. J. Foster, D. P. Lew, M. Herrmann and K.-H. Krause, *Cell. Microbiol.*, 1999, **1**, 101–117.
11 J. K. Ellington, S. S. Reilly, W. K. Ramp, M. S. Smeltzer, J. F. Kellam and M. C. Hudson, *Microb. Pathog.*, 1999, **26**, 317–323.
12 M. Jevon, C. Guo, B. Ma, N. Mordan, S. P. Nair, M. Harris, B. Henderson, G. Bentley and S. Meghji, *Infect. Immun.*, 1999, **67**, 2677–2681.
13 T. J. Foster, *Trends Microbiol.*, 2019, **27**, 927–941.
14 B. Singh, Y.-C. Su and K. Riesbeck, *Mol. Microbiol.*, 2010, **78**, 545–560.
15 B. Singh, Y. Su and K. Riesbeck, *Open Life Sci.*, 2011, **6**(6), 973–980.
16 I. Schvartz, D. Seger and S. Shaltiel, *Int. J. Biochem. Cell Biol.*, 1999, **31**, 539–544.
17 K. Shin, B. C. Lechtenberg, L. M. Fujimoto, Y. Yao, S. S. Bartra, G. V. Plano and F. M. Marassi, *Sci. Adv.*, 2019, **5**, eaax5068.
18 J. I. Fuquay, D. T. Loo and D. W. Barnes, *Infect. Immun.*, 1986, **52**, 714–717.
19 G. S. Chhatwal, K. T. Preissner, G. Müller-Berghaus and H. Blobel, *Infect. Immun.*, 1987, **55**, 1878–1883.
20 O. D. Liang, M. Maccarana, J.-I. Flock, M. Paulsson, K. T. Preissner and T. Wadström, *Biochim. Biophys. Acta, Mol. Basis Dis.*, 1993, **1225**, 57–63.
21 T. Hallström, B. Singh, P. Kraiczy, S. Hammerschmidt, C. Skerka, P. F. Zipfel and K. Riesbeck, *PLoS One*, 2016, **11**, e0147709.
22 O. D. Liang, J.-I. Flock and T. Wadstrom, *J. Biochem.*, 1994, **116**, 457–463.
23 S. Bergmann, A. Lang, M. Rohde, V. Agarwal, C. Rennemeier, C. Grashoff, K. T. Preissner and S. Hammerschmidt, *J. Cell Sci.*, 2009, **122**, 256–267.
24 M. Mahawar and P. Joshi, *Comp. Biochem. Physiol., Part B: Biochem. Mol. Biol.*, 2008, **149**, 410–418.
25 P. Zhuang, A. I. Chen and C. B. Peterson, *J. Biol. Chem.*, 1997, **272**, 6858–6867.
26 C. Sa E Cunha, N. J. Griffiths and M. Virji, *PLoS Pathog.*, 2010, **6**(5), e1000911.
27 F. Lundberg, S. Schliamser and Å. Ljungh, *J. Med. Microbiol.*, 1997, **46**, 285–296.
28 K. P. Haley and E. P. Skaar, *Microbes Infect.*, 2012, **14**, 217–227.
29 J. Sheldon and D. Heinrichs, *Front. Cell. Infect. Microbiol.*, 2012, **2**, 41.
30 J. C. Grigg, G. Ukpabi, C. F. M. Gaudin and M. E. P. Murphy, *J. Inorg. Biochem.*, 2010, **104**, 341–348.
31 G. Pishchany, A. L. McCoy, V. J. Torres, J. C. Krause, J. E. Crowe, M. E. Fabry and E. P. Skaar, *Cell Host Microbe*, 2010, **8**, 544–550.
32 R. M. Corrigan, H. Miajlovic and T. J. Foster, *BMC Microbiol.*, 2009, **9**, 22.
33 H. Miajlovic, M. Zapotoczna, J. A. Geoghegan, S. W. Kerrigan, P. Speziale and T. J. Foster, *Microbiology*, 2010, **156**, 920–928.
34 A. Missineo, A. D. Poto, J. A. Geoghegan, S. Rindi, S. Heilbronner, V. Gianotti, C. R. Arciola, T. J. Foster, P. Speziale and G. Pietrocola, *Infect. Immun.*, 2014, **82**, 2448–2459.
35 M. Zapotoczna, Z. Jevnikar, H. Miajlovic, J. Kos and T. J. Foster, *Cell. Microbiol.*, 2013, **15**, 1026–1041.
36 G. Pietrocola, A. Pellegrini, M. J. Alfeo, L. Marchese, T. J. Foster and P. Speziale, *J. Biol. Chem.*, 2020, **295**, 10008–10022.
37 M. H. Kroll, J. D. Hellums, L. V. McIntire, A. I. Schafer and J. L. Moake, *Blood*, 1996, **88**, 1525–1541.
38 A. Persat, C. D. Nadell, M. K. Kim, F. Ingremeau, A. Siryaporn, K. Drescher, N. S. Wingreen, B. L. Bassler, Z. Gitai and H. A. Stone, *Cell*, 2015, **161**, 988–997.
39 Y. F. Dufrêne and A. Persat, *Nat. Rev. Microbiol.*, 2020, 1–14.
40 M. Otto, *FEMS Microbiol. Rev.*, 2014, **38**, 1250–1270.
41 P. Herman, S. El-Kirat-Chatel, A. Beaussart, J. A. Geoghegan, T. J. Foster and Y. F. Dufrêne, *Mol. Microbiol.*, 2014, **93**, 356–368.
42 P. Herman-Bausier, C. Labate, A. M. Towell, S. Derclaye, J. A. Geoghegan and Y. F. Dufrêne, *Proc. Natl. Acad. Sci. U. S. A.*, 2018, **115**, 5564–5569.
43 P. Vitry, C. Valotteau, C. Feuillie, S. Bernard, D. Alsteens, J. A. Geoghegan and Y. F. Dufrêne, *mBio*, 2017, **8**, e01748.
44 E. Evans, *Annu. Rev. Biophys. Biomol. Struct.*, 2001, **30**, 105–128.

45 R. W. Friddle, A. Noy and J. J. De Yoreo, *Proc. Natl. Acad. Sci. U. S. A.*, 2012, **109**, 13573–13578.
46 M. R. Uhlig, C. A. Amo and R. Garcia, *Nanoscale*, 2018, **10**, 17112–17116.
47 S. R. Clarke, M. D. Wiltshire and S. J. Foster, *Mol. Microbiol.*, 2004, **51**, 1509–1519.
48 L. F. Milles, K. Schulten, H. E. Gaub and R. C. Bernardi, *Science*, 2018, **359**, 1527–1533.
49 C. Schoeler, R. C. Bernardi, K. H. Malinowska, E. Durner, W. Ott, E. A. Bayer, K. Schulten, M. A. Nash and H. E. Gaub, *Nano Lett.*, 2015, **15**, 7370–7376.
50 R. J. Bingham, E. Rudino-Pinera, N. A. G. Meenan, U. Schwarz-Linek, J. P. Turkenburg, M. Hook, E. F. Garman and J. R. Potts, *Proc. Natl. Acad. Sci. U. S. A.*, 2008, **105**, 12254–12258.
51 U. Schwarz-Linek, J. M. Werner, A. R. Pickford, S. Gurusiddappa, J. H. Kim, E. S. Pilka, *et al.*, *Nature*, 2003, **423**(6936), 177–181.
52 J. A. Geoghegan and Y. F. Dufrêne, *Trends Microbiol.*, 2018, **26**, 645–648.
53 T. Vanzieleghem, N. Couniot, P. Herman-Bausier, D. Flandre, Y. F. Dufrêne and J. Mahillon, *Langmuir*, 2016, **32**, 7277–7283.
54 A. Beaussart, S. El-Kirat-Chatel, R. M. A. Sullan, D. Alsteens, P. Herman, S. Derclaye and Y. F. Dufrêne, *Nat. Protoc.*, 2014, **9**, 1049–1055.

